DOI: 10.1002/cphc.200900440

FT Raman and DFT Study on a Series of All-*anti* Oligothienoacenes End-Capped with Triisopropylsilyl Groups

Reyes Malavé Osuna,[a] Víctor Hernández,*[a] Juan T. López Navarrete,*[a] Juan Aragó,[b] Pedro M. Viruela,[b] Enrique Ortí,*[b] Yoshitake Suzuki,[c] Shigehiro Yamaguchi,[c] John T. Henssler,[d] and Adam J. Matzger[d]

Herein, we study the π-conjugational properties of a homologous series of all-*anti* oligothienoacenes containing four to eight fused thiophene rings by means of FT Raman spectroscopy and DFT calculations. The theoretical analysis of the spectroscopic data provides evidence that selective enhancement of a very limited number of Raman scatterings is related to the occurrence in these oligothienoacenes of strong vibronic coupling between collective ν(C=C) stretching modes in the 1600–1300 cm^{-1} region and the HOMO/LUMO frontier orbitals (HOMO = highest occupied molecular orbital; LUMO = lowest unoccupied molecular orbital). The correlation of the Raman spectroscopic data and theoretical results for these all-*anti* oligothienoacenes with those previously collected for a number of all-*syn* oligothienohelicenes gives further support to the expectation that cross-conjugation is dominant in heterohelicenes. Fully planar all-*anti* oligothienoacenes display linear π conjugation which seemingly does not reach saturation with increasing number of annulated thiophene rings in the oligomeric chain at least up to the octamer.

1. Introduction

Acenes are planar organic molecules consisting of aromatic rings fused in a linear fashion. Some acenes, such as pentacene, have been intensely investigated over the past few years as promising organic semiconductors because of their low-lying HOMO (highest occupied molecular orbital) energy levels, which allow for hole injection and strong electronic interactions in the solid state.[1,2] Oligothienoacenes, the fused-ring analogues of α-linked oligothiophenes that resemble acenes, are of particular interest as conjugated materials due to their outstanding electronic properties and environmental stability.[2,3] Because of their rigid architecture, oligothienoacenes are not hampered by the conformational defects in the solid state from which their nonfused counterparts may suffer. Furthermore, oligothiophenes and acenes such as pentacene commonly display a herringbone packing arrangement in the solid state, which is predicted to hinder charge-carrier mobility due to the nonoptimal π–π overlap.[4] In contrast, oligothienoacenes are known to adopt a π-stacked motif in the solid state as a consequence of the relatively high C/H ratio, which reduces the role of C–H···π interactions in the crystal.[5] Despite the highly desirable properties of oligothienoacenes, they have received significantly less attention in the literature over the last decade than α-linked oligothiophenes, perhaps due to the inefficient synthetic routes to their fused-ring architectures.

In recent years, two complementary synthetic methods have been developed which provide efficient and scalable access to oligothienoacenes containing four to eight linearly fused thiophene moieties in an all-*anti* arrangement.[6] Both methods incorporate solubilizing triisopropylsilyl (TIPS) groups at the terminal α positions. These substituents aid in purification and solution processability, and can be removed under mild chemical conditions. For the first time, we have the opportunity to analyze a series of oligothienoacenes to gain insight into the fundamental structure–property relationships with respect to the addition of each ring. Furthermore, this series of compounds can be directly compared to other well-studied series of closely related oligomers, such as nonfused oligothiophenes and fully fused all-*syn* oligothienoacenes.[7]

To gain precise insight into relationships between the structure and properties of a wide range of π-conjugated molecular

[a] *R. Malavé Osuna, Prof. Dr. V. Hernández, Prof. Dr. J. T. López Navarrete*
Department of Physical Chemistry
University of Málaga, 29071 Málaga (Spain)
Fax: (+34) 952-132000
E-mail: hernandez@uma.es
teodomiro@uma.es

[b] *J. Aragó, Prof. Dr. P. M. Viruela, Prof. Dr. E. Ortí*
Instituto de Ciencia Molecular, Universidad de Valencia
P.O. Box 22085, 46071 Valencia (Spain)
Fax: (+34) 963543274
E-mail: enrique.orti@uv.es

[c] *Prof. Dr. Y. Suzuki, Prof. Dr. S. Yamaguchi*
Department of Chemistry, Graduate School of Science
Nagoya University, Furo, Chikusa, Nagoya, 464-8602 (Japan)

[d] *Prof. Dr. J. T. Henssler, Prof. Dr. A. J. Matzger*
Department of Chemistry and the Macromolecular Science and Engineering Program, University of Michigan
930 North University, Ann Arbor, Michigan 48109-1055 (USA)

Supporting information for this article is available on the WWW under http://dx.doi.org/10.1002/cphc.200900440.

architectures, Raman spectroscopy has been proved to be an important tool. For example, experimental observables such as Raman frequencies and intensities are closely related to the π-conjugational properties of oligothiophenes and related systems, which account for their main optical and electronic signatures. The well-established effective conjugation coordinate (ECC) model[8] predicts two main trends of variation for the Raman spectral fingerprints of π-conjugated molecules: 1) selective enhancement of particular scatterings associated with collective C=C/C–C stretching vibrations of the π-conjugated backbone (related to the existence in this type of one-dimensional systems of an electron–phonon coupling mechanism which is at the origin of their exceptional optical and electrical properties) and 2) frequency downshift of these enhanced Raman bands on relaxation of the molecular structure as a consequence of either greater π-electron conjugation in the neutral state or quinoidization induced by ionization. However, it has been experimentally demonstrated that, for oligothiophenes, although the increase in conjugation results in a downward frequency shift of the Raman-active modes, close intermolecular interactions of the π frameworks cause a competing upward shift.[9] Therefore, the very bulky TIPS groups, which reduce or eliminate interactions between the π frameworks, are an important structural feature of the compounds in this study. Combination of these experimental spectroscopic data with reliable quantum chemical calculations allows precise assessment of relevant molecular parameters which would be very difficult to evaluate by other conventional experimental techniques. Due to implementation of electron-correlation effects, first-principles quantum chemical calculations in the framework of density functional theory (DFT) are well-suited to modeling extended π-conjugated molecular architectures.

Herein, a homologous series of oligothienoacenes[6] having four to eight fused thiophene rings is analyzed by Raman spectroscopy and DFT//B3LYP/6-31G** calculations to determine why some Raman scatterings of annulated systems become selectively intensified. The atomic displacements calculated for each molecular vibration and the electronic density contours computed for the frontier molecular orbitals (HOMO and LUMO, lowest unoccupied molecular orbital) are compared. These data demonstrate that the Raman features particularly enhanced in the 1600–1300 cm^{-1} spectral region correspond to totally symmetric ν(C=C) stretching modes strongly coupled with the HOMO and LUMO wave functions. The strongest bands observed in the Raman spectra are those largely decreasing the LUMO energy and leading to simultaneous HOMO destabilization.

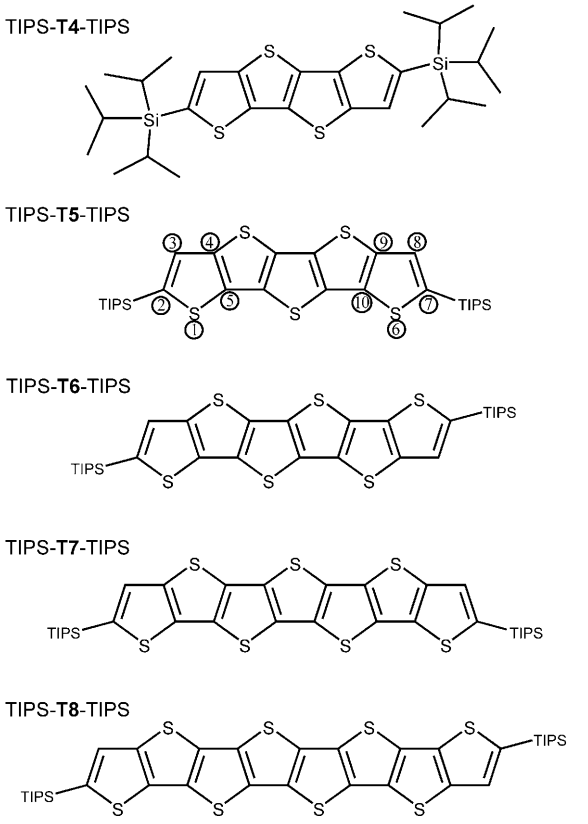

Figure 1. Chemical structures of the oligothienoacenes TIPS-**T*n***-TIPS (TIPS: triisopropylsilyl) under study. The atom numbering used in the text for TIPS-**T5**-TIPS is given.

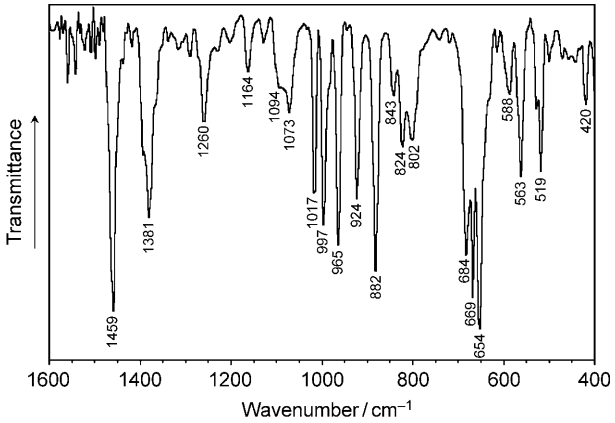

Figure 2. FTIR spectrum of TIPS-**T7**-TIPS in the 1600–400 cm^{-1} range.

2. Results and Discussion

The chemical structures of the end-capped oligothienoacenes under study (TIPS-**T*n***-TIPS, where *n* indicates the number of fused thiophene rings) are displayed in Figure 1. The experimental solid-state FTIR spectral profile for TIPS-**T7**-TIPS and the FT Raman spectral profiles for the entire series of oligothienoacenes are shown in Figures 2 and 3, respectively. Figure 4 illustrates how some Raman-active vibrations appearing between 1500 and 1200 cm^{-1} are selectively enhanced with respect to the many Raman scatterings experimentally recorded below 1200 cm^{-1}. On the contrary, the IR absorption spectral profile is much more complex and several features are recorded with similar intensities in the frequency range between 1500 and 400 cm^{-1}. As sketched in Figure 5, most of these vibrations arise from the triisopropylsilyl end-capping groups or from in-plane, but nontotally symmetric, skeletal vibrations of the annulated oligothienyl framework, which give rise to the largest variations in the molecular dipole moment. Only the vi-

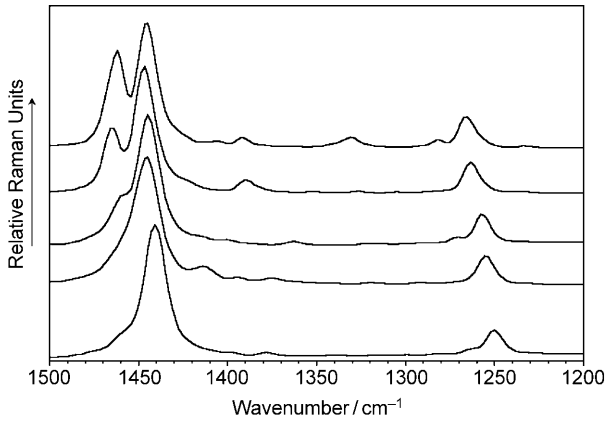

Figure 3. Solid-state FT Raman spectra of the whole series of oligothienoacenes in the 1500–1200 cm^{-1} range. The Nd:YAG laser excitation wavelength λ_{exc} was 1064 nm. Spectral profiles displayed from top to bottom correspond to shorter (TIPS-**T4**-TIPS) to longer (TIPS-**T8**-TIPS) oligomers.

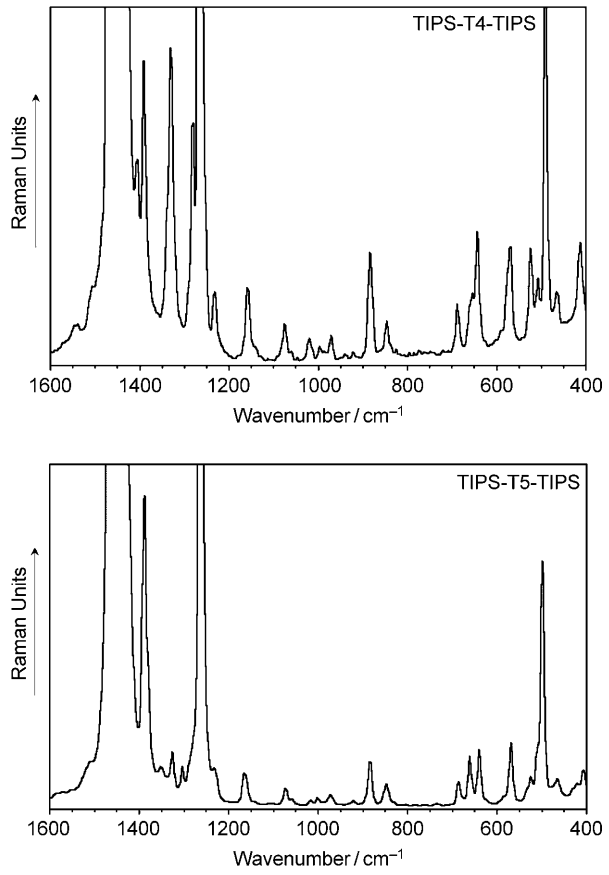

Figure 4. Enlarged profiles of the solid-state FT Raman spectra of TIPS-**T4**-TIPS (top) and TIPS-**T5**-TIPS (bottom) illustrating more precisely the selective enhancement with increasing chain length of a very limited number of Raman scatterings between 1600 and 1200 cm^{-1}, as opposed to the many Raman-active molecular vibrations recorded with lower intensity below 1200 cm^{-1}.

brational mode at 1381 cm^{-1} shows a sizeable coupling with the π-conjugated degree of freedom, whereas most the remaining IR-active normal modes display negligible coupling to the π-conjugation pathway.

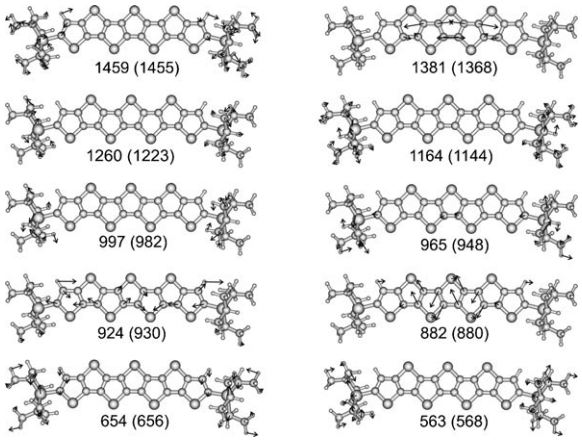

Figure 5. B3LYP/6-31G** vibrational eigenvectors calculated for some of the strongest IR bands of TIPS-**T7**-TIPS. Experimental and theoretical (in parentheses) wavenumbers are given in reciprocal centimeters.

Raman spectral analysis has already been reported for several types of π-conjugated materials including systems with rather complex molecular architectures and substitution patterns.[10] However, the majority of previous studies focus on different homologous series of α-linked oligoheterocycles, with linear or cyclic arrangements of the successive π-conjugated rings, but not on annulated systems such as acenes or heteroacenes. Despite the increasing attention paid to these conjugated fused-ring systems for organic electronic applications, only a relatively small amount of Raman scattering data is available.

The effective conjugation coordinate (ECC) formalism, developed by Zerbi and co-workers, is a method of interpreting Raman experimental observations which implicitly formulates the existence of a unique collective C=C/C–C stretching mode largely involved in the electron–phonon coupling mechanism inherent to these kinds of one-dimensional π-conjugated systems.[8] In aromatic or heteroaromatic polyconjugated chains, the so-called ECC vibrational coordinate has the analytic form of a linear combination of ring C=C/C–C stretching modes, which belongs to the totally symmetric species and points towards the direction of a structural evolution of the π-conjugated framework from a benzenoid pattern (usually that of the ground electronic state) to a quinoid one (that corresponding to the excited electronic state). The ECC model states that the totally symmetric skeletal C=C/C–C stretching vibrations mostly involved in the lattice dynamics of this collective ECC coordinate (i.e., those which give rise to the few selectively enhanced Raman scatterings) should experience significant dispersions both in peak positions and intensities with increasing the size of the π-conjugated backbone within a given series of neutral oligomers. In this regard, experimental detection of changes in Raman frequencies and intensities with variable chain length constitutes a very useful way to evaluate the effectiveness of the π conjugation for a particular family of α-linked oligoheteroaromatics. Additionally, on chemical or electrochemical doping of these π-conjugated α-oligoheterocycles, various types of quinoid-like charged species are created.[11]

The increasing quinoidization of the π-conjugated backbone on progressive injection or removal of a first, second, third electron, and so on also gives rise to a steady redshift of the overwhelmingly strong Raman scatterings due to continuous softening of the polyconjugated path of C=C bonds. This spectroscopic Raman information is quite valuable in elucidating the kind and size of the charge carriers resulting from the various redox processes (i.e., radical cations or anions, dications, dianions, and so on).[12–15]

Figure 6 presents the B3LYP/6-31G** Raman spectra calculated for the TIPS-T*n*-TIPS oligothienoacenes. The theoretical spectra reasonably match the experimental data in peak positions, but relative intensities are less accurately reproduced by computations (compare Figures 3 and 6). As displayed in Figure 7, the vibrational eigenvectors related to the strongest Raman scatterings of these end-capped oligothienoacenes are consistent with the assumption that the selectively enhanced Raman lines arise from similar skeletal ν(C=C) stretching modes. As can be inferred from the minimum-energy, B3LYP/6-31G**-optimized geometries, (Table S1 in the Supporting Information), the π-conjugated C=C bonds forming the carbon skeleton become progressively softened with increasing number of fused thiophene rings, and such softening also vary within each oligothienoacene, reaching its maximum for the C=C bonds of the central thiophene rings.

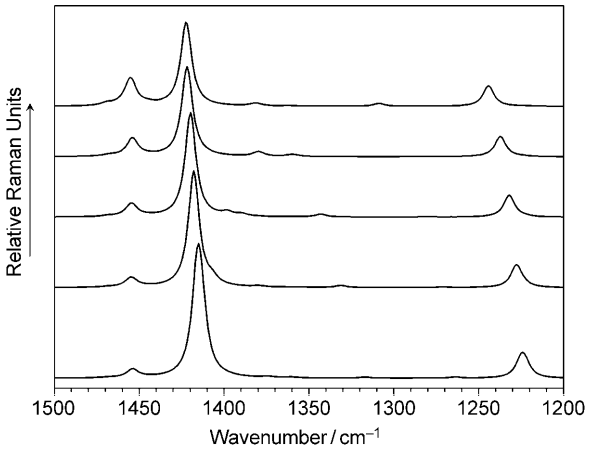

Figure 6. B3LYP/6-31G** Raman profiles calculated for all the oligothienoacenes under study. Spectral profiles displayed from top to bottom correspond to shorter (TIPS-**T4**-TIPS) to longer (TIPS-**T8**-TIPS) oligomers.

As an example of a shorter thienoacene in the series, the Raman spectrum of TIPS-**5T**-TIPS is analyzed in detail. The most intense band, observed at 1447 cm^{-1}, corresponds to the collective ν(C=C) stretching mode calculated at 1422 cm^{-1}, which strongly couples with both the HOMO and the LUMO frontier molecular orbitals (Figure 8). On distortion of TIPS-**T5**-TIPS along the 1447 cm^{-1} Raman-active vibrational mode in the same direction as shown in Figure 7, the strong C_β–C_β bond displacements, along with the small variations in C_α–C_β bond length, cause an increase of the bonding (antibonding) C_β–C_β interactions of the LUMO (HOMO), with the result that the LUMO (HOMO) along this molecular vibration is significantly stabilized (destabilized) in energy. Therefore, the HOMO–LUMO energy gap is narrowed along the Raman mode of 1447 cm^{-1}. Distortion of TIPS-**T5**-TIPS along the 499 cm^{-1} in-plane bending (Figures 4, bottom and 7) results in the antibonding interactions (LUMO) between the S and C_α atoms becoming weaker, particularly for the innermost rings (see Figure 8). Similarly, this 499 cm^{-1} distortion causes slight weakening of the small bonding interactions (HOMO) between the S atoms at both ends of the oligothienyl chain and the adjacent C_α atoms. Therefore, a downshift in energy is expected for the LUMO while a slight upshift occurs in the HOMO for the Raman-active 499 cm^{-1} mode.

The intense Raman peak observed at 1465 cm^{-1} (Figure 3) for TIPS-**T5**-TIPS is due to the vibrational mode calculated at 1454 cm^{-1}, which mainly involves the TIPS groups but also implies antisymmetric stretching of the C_α–C_β bonds of the outermost thiophene rings (Figure 7). Along the 1465 cm^{-1} Raman-active mode, the bonding C(2)–C(3) and C(7)–C(8) interactions in the HOMO are strengthened, but the bonding C(4)–C(5) and C(9)–C(10) ones are softened to a minor extent. The same "competition" occurs with regard to the corresponding antibonding interactions in the LUMO. Therefore, the LUMO (HOMO) is slightly stabilized (destabilized) in energy along this molecular vibration. This is the reason why the ν_{asym}(C=C) stretching of the terminal fused thiophene rings

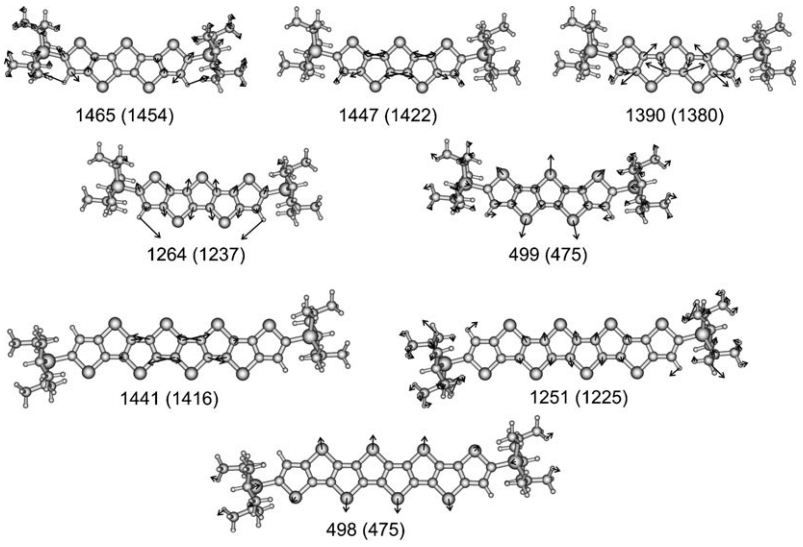

Figure 7. B3LYP/6-31G** vibrational eigenvectors associated with the most outstanding Raman features of TIPS-**T5**-TIPS (top) and TIPS-**T8**-TIPS (bottom). Experimental and theoretical (in parentheses) wavenumbers are expressed in reciprocal centimeters.

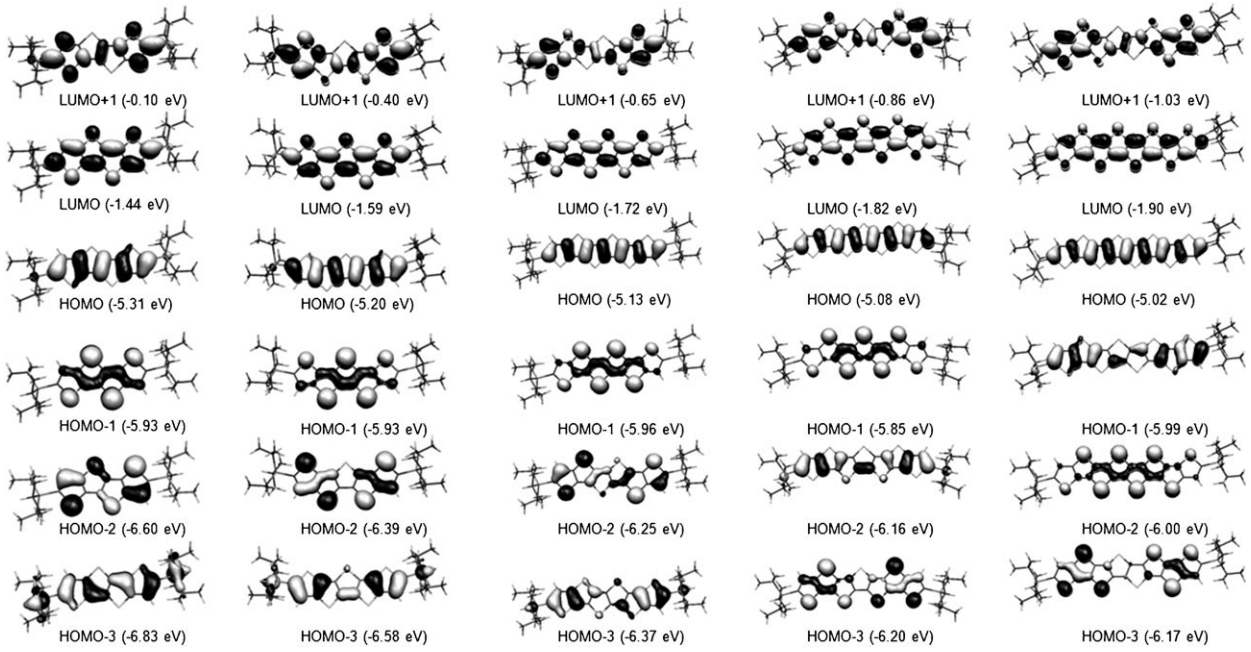

Figure 8. B3LYP/6-31G** electronic density contours (0.03 e bohr^{-3}) and energies for selected MOs around the band-gap region along the whole series of oligothienoacenes.

measured at 1465 cm^{-1} is less coupled to both the HOMO and the LUMO than the collective ν_{sym}(C=C) mode of 1447 cm^{-1}, which spreads over the whole π framework of conjugated double bonds. Regarding the medium-intensity Raman line recorded for TIPS-**T5**-TIPS at 1390 cm^{-1} (Figures 3 and 4, bottom), now we see that the structural distortion of the π-framework along the direction depicted in Figure 7 significantly weakens the antibonding (LUMO) and bonding (HOMO) interactions between the four pairs of C_α and C_β atoms at both of the terminal fused thiophene rings, whereas for the middle ring of the pentathienoacene both types of interactions give the opposite effect. These are the reasons why the HOMO–LUMO gap is narrowed in energy to a lesser extent along the Raman mode of 1390 cm^{-1} in comparison to the two ν(C=C) stretching vibrations giving rise to the strongest Raman features at 1447 and 1465 cm^{-1}.

Notably, a medium-intensity Raman band which is observed in TIPS-**T5**-TIPS but has no counterpart in common linear α-linked oligothiophenes is found at 1264 cm^{-1} (Figures 3 and 4, bottom). This band is attributed to the totally symmetric δ_{sym}(CC) in-plane bending motion calculated at 1237 cm^{-1}, which is primarily located on the inner annulated thienyl rings (Figure 7). The Raman activity of this particular band is enhanced on introduction of electron-rich sulfur bridges in place of β-protons. The structural changes taking place along this collective molecular vibration look like those occurring in the π-conjugated system on HOMO$\rightarrow$LUMO excitation. Furthermore, the strongest Raman lines at 1465 and 1447 cm^{-1} are recorded at lower wavenumbers in the oligothienoacenes than in their α-linked analogues with the same number of double bonds. For example, the strongest Raman scatterings of α-terthiophene are recorded at 1530 and 1460 cm^{-1}. This molecular signature of the improved π conjugation in the fused systems, which also suggests a softer and more easily polarizable π-conjugated framework, is due to the increased number of sulfur atoms.

As the number of fused thiophene rings increases, the Raman spectrum undergoes a progression that is indicative of the expanding π conjugation (Figure 3). TIPS-**T8**-TIPS was analyzed in great detail to reveal the character of an oligomer at the longer end of the thienoacene series under study. The Raman spectrum of TIPS-**T8**-TIPS shows only three main peaks at 1441, 1251, and 498 cm^{-1}, in spite of the very large number of Raman-active vibrations predicted by the optical selection rules. Correlation of the B3LYP/6-31G** Raman-active vibrational eigenvectors (Figure 7) and the electronic density contours related to the frontier MOs of TIPS-**T8**-TIPS (Figure 8) provides an explanation for these experimental findings. Considering C_β–C_β and C_α–C_β interactions (analogous to those of TIPS-**T5**-TIPS) of the four innermost thiophene rings, distortion of TIPS-**T8**-TIPS in the same direction as the Raman-active mode of 1441 cm^{-1} leads to stronger bonding and antibonding interactions in the LUMO and HOMO, respectively. Hence, the LUMO becomes stabilized whereas the HOMO is destabilized along such a collective molecular vibration, as expected for a large vibronic coupling.

On structural relaxation of TIPS-**T8**-TIPS along the in-plane bending of 498 cm^{-1} (Figure 7), the antibonding interactions in the LUMO between the five innermost sulfur atoms and their adjacent C_α atoms become weaker (Figure 8), and thus a downshift in energy of the LUMO occurs, whereas the vibronic coupling of this Raman mode to the corresponding HOMO is negligible in this case.

Finally, the Raman band of TIPS-**T8**-TIPS at 1251 cm^{-1} is correlated with that of TIPS-**T4**-TIPS at 1266 cm^{-1}. It undergoes the largest downward dispersion among all Raman scatterings on increasing the number of annulated thiophene units in the oligomeric chain in the series of thienoacenes in this study. Its associated eigenvector (Figure 7) reveals that this selectively enhanced Raman line must be ascribed to a totally symmetric δ_{sym}(C–C) in-plane bending mainly located on the four innermost fused thienyl units. The band has no counterpart in nonfused α-linked oligothiophenes but arises on bridging of all the interior C_β atoms of the π-conjugated frame by electron-rich sulfur atoms.

Across the entire series of oligothiophenes in this study, there is a redshift in the strongest Raman scatterings as the number of fused thiophene units increases. This phenomenon is more clearly observed for the Raman-active modes in the 1251–1266 cm^{-1} region, as described above and shown in Figure 3. This trend is well correlated with the theoretical DFT (B3LYP/6-31G**) predictions shown in Figure 6. The lower wavenumbers observed in the theoretical spectra are due to the well-known overestimation of π conjugation by this method. These data suggest that even TIPS-**T8**-TIPS has not yet reached saturation length and it is predicted that greater π conjugation may be achieved across the planar molecular architecture by construction of thienoacenes with more than eight fused thiophene rings.

Examination of the frontier molecular orbital topologies (Figure 8) provides further insight into the differences between oligothienoacenes and their α-linked analogues. For example, in α-linked oligothiophenes there is very little contribution from the sulfur atoms to the π system for both the doubly occupied and empty MOs around the band-gap region, whereas in oligothienoacenes the sulfur atoms make a significant contribution to these orbitals. This observation is particularly evident in the case of the HOMO−1 and HOMO−2 of the three shorter oligothienoacenes; HOMO−1, HOMO−3, and HOMO-4 of TIPS-**T7**-TIPS; and HOMO−2, HOMO−3, and HOMO−4 of TIPS-**T8**-TIPS. This is attributed to the rigidly planar π framework of unsaturated C_{sp2} atoms, which includes the electron-rich and easily polarizable sulfur atoms. However, this electronic feature cannot be merely viewed as a result of the arrangement of successive fused thiophene rings in an all-*anti* fashion, which leads to heteroacenes for which an overall path of linear π conjugation along the main molecular axis can be formulated, because similar behavior has been previously noted in some quaterthienoacenes arranged in a non-all-*anti* fashion and for helically annulated all-*syn* oligothiophenes, that is, heteroacenes for which cross-conjugation is an increasing or main factor.[7b,c]

The topologies of the frontier molecular orbitals (B3LYP/6-31G**) around the band-gap region for these all-*anti* oligothienoacenes reveal notable differences in comparison to those of closely related oligothienoacenes which are oriented in an all-*syn* fashion. The overall patterns of the atomic coefficients for the frontier MOs in the all-*syn* 7-mer are quite similar to those of the all-*syn* 3-mer, that is, they are largely localized on the three central thiophene rings of the 7-mer.[7b] This is in strong contrast to what is found for the all-*anti* series of TIPS-**T*n***-TIPS, whose frontier MOs spread over the whole π framework of fully planar annulated thiophenes (see Figure 8). This behavior and the finding that enhanced Raman scatterings appear more disperse with increasing number of the annulated thiophene rings in the all-*anti* TIPS-**T*n***-TIPS series as compared to their all-*syn* oligothienyl counterparts suggest significant electron localization in the latter conformation relative to the former. In other words, all-*syn* fused β-oligothiophenes may be regarded as being mostly cross-conjugated in nature, in spite of sizeable contributions from sulfur atoms to the frontier MOs, whereas all-*anti* TIPS-**T*n***-TIPS oligothienoacenes clearly exhibit linear π conjugation.

3. Conclusions and Outlook

We have studied the conjugational properties of a homologous series of all-*anti* oligothienoacenes having four to eight fused thiophene rings by means of FT Raman spectroscopy and DFT calculations. Selective enhancement of a very limited number of Raman scatterings among the many Raman-active molecular vibrations predicted by the optical selection rules is related to strong vibronic coupling between selected skeletal ν(C=C) stretching modes in the 1600–1300 cm^{-1} range and the HOMO/LUMO frontier orbitals. The strongest Raman features are assigned in all cases to particular skeletal vibrations, with a marked collective character, along which the displacements of the carbon or sulfur atoms from their equilibrium positions better match the orientations of the bonding/antibonding interactions in the HOMO/LUMO orbital patterns, which thus lead to pronounced narrowing of the HOMO–LUMO energy gap. Theoretical B3LYP/6-31G** wave functions for the MOs around the band-gap region also reveal the essential role played in these heteroacenes by the many electron-rich sulfur atoms surrounding the π-conjugated backbone. In this regard, all-*anti* oligothienoacenes are found to display rather different atomic orbital compositions for the higher occupied molecular orbitals (i.e., HOMO−1, HOMO−2, and so on) compared to their α-linked oligothiophene counterparts with the same number of π-conjugated C=C bonds, for which the carbon backbone mainly contributes. Comparison of the Raman data and the B3LYP/6-31G** results collected for these all-*anti* oligothienoacenes with those previously obtained for a number of all-*syn* oligothienohelicenes gives further support to the conclusion that cross-conjugation is dominant in the latter systems, whereas all-*anti* oligothienoacenes clearly display linear π conjugation along the main molecular axis. π conjugation in all-*anti* oligothienoacenes seemingly does not reach saturation in this homologous series of increasing chain lengths up to the octamer TIPS-**T8**-TIPS.

Experimental and Computational Methods

The synthesis and purification of the oligothienoacenes are described elsewhere.[6] FTIR spectra were recorded on a Bruker Equinox 55 spectrometer. Compounds were ground to powder and pressed in KBr pellets. FTIR spectra with a standard spectral resolution of

2 cm^{-1} were collected as the average of 50 scans. Interference from atmospheric water vapor was minimized by purging the instrument with dry argon before starting data collection. FT Raman scattering spectra were collected on a Bruker FRA106/S apparatus with Nd:YAG laser source ($\lambda_{exc} = 1064$ nm) in a backscattering configuration. The operating power for the exciting laser radiation was kept to 100 mW in all experiments. Samples were analyzed as pure solids in sealed capillaries. Typically, 1000 scans with 2 cm^{-1} spectral resolution were averaged to optimize the signal-to-noise ratio.

Density functional theory (DFT) calculations were carried out using the Gaussian 03 program suite[16] running on a cluster of Intel Xeon Quad Core CPUs. Becke's three-parameter exchange functional combined with the LYP correlation functional (B3LYP)[17] was employed, because it has been shown that the B3LYP functional yields similar geometries for medium-sized molecules to MP2 calculations with the same basis sets.[18,19] Moreover, the DFT force fields calculated with the B3LYP functional yield infrared spectra in very good agreement with experiment.[20–22] The standard 6-31G** basis set was used to obtain optimized geometries on isolated entities.[23] Appropriate symmetry constraints [C_i (C_2) for oligomers with an even (odd) number of fused thiophene rings] were imposed during geometry optimization of each system while allowing all geometrical parameters of half the molecule to vary independently. On the resulting ground-state optimized geometries, harmonic vibrational frequencies and infrared and Raman intensities were calculated with the B3LYP functional.

We used the often-practiced adjustment of the theoretical force fields in which calculated harmonic vibrational frequencies are uniformly scaled down by a factor of 0.96 for B3LYP/6-31G** calculations.[20,22] This scaling procedure is often accurate enough to disentangle serious experimental misassignments. All vibrational frequencies reported here are thus-scaled values. The theoretical Raman spectra were obtaining by convoluting the scaled frequencies with Gaussian functions (10 cm^{-1} width at half-height). The relative heights of the Gaussians were determined from the theoretical Raman scattering activities. Molecular orbital contours were plotted by using Molekel 4.3.[24]

Acknowledgements

Financial support by the Ministerio de Educación y Ciencia (MEC) of Spain (projects CTQ2006-14987-C02-01 and CTQ2006-14987-C02-02 and Consolider-Ingenio CSD2007-00010 in Molecular Nanoscience), the Junta de Andalucia (grant FQM-0159), the Generalitat Valenciana (grant ACOMP/2009/269), and European FEDER funds (project CTQ2006-14987-C02) are greatly acknowledged. R.M.O. and J.A. are also grateful to the MEC for personal doctoral grants.

Keywords: acenes · computational chemistry · conjugation · density functional calculations · Raman spectroscopy

[1] J. E. Anthony, *Angew. Chem.* **2008**, *120*, 460–492; *Angew. Chem. Int. Ed.* **2008**, *47*, 452–483.
[2] A. R. Murphy, J. M. J. Frechet, *Chem. Rev.* **2007**, *107*, 1066–1096.
[3] T. Torroba, M. García-Valverde, *Angew. Chem.* **2006**, *118*, 8270–8274; *Angew. Chem. Int. Ed.* **2006**, *45*, 8092–8096.
[4] J. L. Brédas, J. P. Calbert, D. A. da Silva, J. Cornil, *Proc. Natl. Acad. Sci. USA* **2002**, *99*, 5804–5809.
[5] a) X. Zhang, A. J. Matzger, *J. Org. Chem.* **2003**, *68*, 9813–9815; b) G. R. Desiraju, A. Gavezzotti, *Acta Crystallogr. Sect. B* **1989**, *45*, 473–482; c) A. Gavezzotti, G. R. Desiraju, *Acta Crystallogr. Sect. B* **1988**, *44*, 427–434.
[6] a) X. Zhang, A. P. Côté, A. J. Matzger, *J. Am. Chem. Soc.* **2005**, *127*, 10502–10503; b) T. Okamoto, K. Kudoh, A. Wakamiya, S. Yamaguchi, *Chem. Eur. J.* **2007**, *13*, 548–556.
[7] a) R. Malavé Osuna, R. Ponce Ortiz, V. Hernández, J. T. López Navarrete, M. Miyasaka, S. Rajca, A. Rajca, R. Glaser, *J. Phys. Chem. C* **2007**, *111*, 4854–4860; b) R. Malavé Osuna, R. Ponce Ortiz, M. C. Ruiz Delgado, V. G. Nenajdenko, V. V. Sumerin, E. S. Balenkova, V. Hernández, J. T. López Navarrete, *ChemPhysChem* **2007**, *8*, 745–750; c) V. Hernández, J. Casado, F. J. Ramirez, G. Zotti, S. Hotta, J. T. López Navarrete, *J. Chem. Phys.* **1996**, *104*, 9271–9282; d) J. Casado, S. Hotta, V. Hernández, J. T. López Navarrete, *J. Phys. Chem. A* **1999**, *103*, 816–822.
[8] a) G. Zerbi, C. Castiglioni, M. Del Zoppo, *Electronic Materials: The Oligomer Approach*, Wiley-VCH, Weinheim, **1998**; b) C. Castiglioni, M. Gussoni, J. T. López Navarrete, G. Zerbi, *Solid State Commun.* **1988**, *65*, 625–630; c) J. T. López Navarrete, G. Zerbi, *J. Chem. Phys.* **1991**, *94*, 957–964; d) V. Hernández, C. Castiglioni, M. Del Zoppo, G. Zerbi, *Phys. Rev. B* **1994**, *50*, 9815–9823; e) E. Agosti, M. Rivola, V. Hernández, M. Del Zoppo, G. Zerbi, *Synth. Met.* **1999**, *100*, 101–112; f) G. Zerbi, *Handbook of Conducting Polymers*, Marcel Dekker, New York, **1998**.
[9] A. Milani, L. Bambrilla, M. Del Zoppo, G. Zerbi, *J. Phys. Chem. B* **2007**, *111*, 1271–1276.
[10] a) M. C. Ruiz Delgado, J. Casado, V. Hernández, J. T. López Navarrete, G. Fuhrmann, P. Bauerle, *J. Phys. Chem. B* **2004**, *108*, 3158–3167; b) J. Casado, V. Hernández, R. Ponce Ortiz, M. C. Ruiz Delgado, J. T. López Navarrete, G. Fuhrmann, P. Bauerle, *J. Raman Spectrosc.* **2004**, *35*, 592–599.
[11] a) Ch. Ehrendorfer, A. Karpfen, *J. Phys. Chem.* **1994**, *98*, 7492–7496; b) Ch. Ehrendorfer, A. Karpfen, *J. Phys. Chem.* **1995**, *99*, 5341–5353.
[12] A. Sakamoto, Y. Furukawa, M. Tasumi, *J. Phys. Chem.* **1994**, *98*, 4635–4640.
[13] a) N. Yokonuma, Y. Furukawa, M. Tasumi, M. Kuroda, J. Nakayama, *Chem. Phys. Lett.* **1996**, *255*, 431–436; b) I. Harada, Y. Furukawa, *Vibrational Spectra and Structure, Vol. 19* (Ed.: J. Durig), Elsevier, Amsterdam, **1991**.
[14] a) C. Moreno Castro, M. C. Ruiz Delgado, V. Hernández, S. Hotta, J. Casado, J. T. López Navarrete, *J. Chem. Phys.* **2002**, *116*, 10419–10427; b) C. Moreno Castro, M. C. Ruiz Delgado, V. Hernández, Y. Shirota, J. Casado, J. T. López Navarrete, *J. Phys. Chem. B* **2002**, *106*, 7163–7170; c) M. C. Ruiz Delgado, V. Hernández, J. T. López Navarrete, S. Tanaka, Y. Yamashita, *J. Phys. Chem. B* **2004**, *108*, 2516–2526; d) J. Casado, R. Ponce Ortiz, M. C. Ruiz Delgado, R. Azumi, R. T. Oakley, V. Hernández, J. T. López Navarrete, *J. Phys. Chem. B* **2005**, *109*, 10115–10125.
[15] a) J. Casado, V. Hernández, S. Hotta, J. T. López Navarrete, *J. Chem. Phys.* **1998**, *109*, 10419–10429; b) J. Casado, V. Hernández, S. Hotta, J. T. López Navarrete, *Adv. Mater.* **1998**, *10*, 1458–1461; c) J. Casado, L. L. Miller, K. R. Mann, T. M. Pappenfus, Y. Kanemitsu, E. Ortí, P. M. Viruela, P. Pou-Amérigo, V. Hernández, J. T. López Navarrete, *J. Phys. Chem. B* **2002**, *106*, 3872–3881; d) J. Casado, L. L. Miller, K. R. Mann, T. M. Pappenfus, V. Hernández, J. T. López Navarrete, *J. Phys. Chem. B* **2002**, *106*, 3597–3605; e) J. Casado, M. C. Ruiz Delgado, Y. Shirota, V. Hernández, J. T. López Navarrete, *J. Phys. Chem. B* **2003**, *107*, 2637–2644.
[16] Gaussian 03 (Revision B.04), M. J. Frisch, G. W. Trucks, H. B. Schlegel, G. E. Scuseria, M. A. Robb, J. R. Cheeseman, J. A. Montgomery, Jr., T. Vreven, K. N. Kudin, J. C. Burant, J. M. Millam, S. S. Iyengar, J. Tomasi, V. Barone, B. Mennucci, M. Cossi, G. Scalmani, N. Rega, G. A. Petersson, H. Nakatsuji, M. Hada, M. Ehara, K. Toyota, R. Fukuda, J. Hasegawa, M. Ishida, T. Nakajima, Y. Honda, O. Kitao, H. Nakai, M. Klene, X. Li, J. E. Knox, H. P. Hratchian, J. B. Cross, C. Adamo, J. Jaramillo, R. Gomperts, R. E. Stratmann, O. Yazyev, A. J. Austin, R. Cammi, C. Pomelli, J. W. Ochterski, P. Y. Ayala, K. Morokuma, G. A. Voth, P. Salvador, J. J. Dannenberg, V. G. Zakrzewski, S. Dapprich, A. D. Daniels, M. C. Strain, O. Farkas, D. K. Malick, A. D. Rabuck, K. Raghavachari, J. B. Foresman, J. V. Ortiz, Q. Cui, A. G. Baboul, S. Clifford, J. Cioslowski, B. B. Stefanov, G. Liu, A. Liashenko, P. Piskorz, I. Komaromi, R. L. Martin, D. J. Fox, T. Keith, M. A. Al-Laham, C. Y. Peng, A. Nanayakkara, M. Challacombe, P. M. W. Gill, B. Johnson, W. Chen, M. W. Wong, C. Gonzalez, J. A. Pople, Gaussian Inc., Pittsburgh, PA, **2003**.
[17] A. D. Becke, *J. Chem. Phys.* **1993**, *98*, 1372–1377.

[18] a) P. J. Stephens, F. J. Devlin, F. C. F. Chabalowski, M. J. Frisch, *J. Phys. Chem.* **1994**, *98*, 11623–11627; b) J. J. Novoa, C. Sosa, *J. Phys. Chem.* **1995**, *99*, 15837–15845.
[19] P. M. Viruela, R. Viruela, E. Ortí, *Int. J. Quantum Chem.* **1998**, *70*, 303–312.
[20] A. P. Scott, L. Radom, *J. Phys. Chem.* **1996**, *100*, 16502–16513.
[21] G. Rauhut, P. Pulay, *J. Phys. Chem.* **1995**, *99*, 3093–3100.
[22] C. A. Jiménez-Hoyos, B. J. Janesko, G. E. Scuseria, *Phys. Chem. Chem. Phys.* **2008**, *10*, 6621–6629.
[23] M. M. Francl, W. J. Pietro, W. J. Hehre, J. S. Binkley, M. S. Gordon, D. J. Defrees, J. A. Pople, *J. Chem. Phys.* **1982**, *77*, 3654–3665.
[24] S. Portmann, H. P. Lüthi, *Chimia* **2000**, *54*, 766–770.

Received: June 8, 2009
Revised: July 23, 2009
Published online on October 6, 2009

